On the influence of drained cyclic preloadings on the cyclic behaviour of Zbraslav sand

J. Duque [a,b,*], J. Roháč [a], D. Mašín [a]

[a] *Charles University, Prague, Czech Republic*
[b] *Universidad de la Costa, Barranquilla, Colombia*

ARTICLE INFO

ABSTRACT

This article experimentally evaluates the influence of directional drained cyclic preloadings on the subsequent undrained monotonic and cyclic response of Zbraslav sand. The cyclic tests were performed on dense samples and under triaxial conditions. The experiments considered several different preloading directions, magnitude of the maximum deviatoric stress reached during the drained preloading stage and deviatoric stress amplitudes during the undrained shearing stage. The experimental results suggested that the rate of strains and pore water pressure accumulation, and therefore, the number of cycles to reach initial liquefaction or failure conditions are remarkably affected by the direction of the drained preloading history. In addition, the preloading direction plays a major role on the contractive/dilative response during the subsequent undrained monotonic loading. In particular, directional drained cyclic preloadings toward positive deviatoric stresses at constant mean effective stress and isotropic compression led to more dilative responses. Contrary, preloadings toward negative deviatoric stresses at constant mean effective stress led to more contractive responses. The results suggest that these major variations cannot be associated to the rather small changes in the relative density of the samples but likely due to fabric changes and induced anisotropy caused by the drained preloading history.

1. Introduction

Different factors may induce preloading histories in in-situ sand deposits due to changes in the stress states via different stress paths. For instance, new excavations or tunnelling may lead to unloading stress states which can be followed by refilling, compaction and construction of overlying structures (loading stages). The aforementioned unloading/loading stages modify the subsequent soil mechanical behaviour, and therefore, the ground deformations and liquefaction resistance [1–6]. Actually, several laboratory experiments have shown that former loading/unloading episodes strongly affect the subsequent soil mechanical behaviour, effect which is usually denoted as stress–strain history [7–14]. Therefore, in order to accurately understand and predict the soil behaviour, a proper understanding and reproduction of the influence of the stress–strain history on the subsequent soil mechanical behaviour is necessary.

Among the first research dealing with the influence of monotonic preloadings on the subsequent monotonic behaviour of granular soils are the works performed by Finn et al. [15], Lee & Albaisa [16], Toki & Kitago [17] and Ishihara & Okada [18,19]. They reported that the application of preloadings remarkably impact the subsequent liquefaction resistance. After that, several subsequent works extended the literature

by considering monotonic triaxial preloadings but different soil types, densities, stress states, and magnitude of the preloadings, among many other relevant variables e.g. [6,20–35]. The main limitation of the aforementioned works, and most works related to preloadings in the literature, is that they are just focused on the influence of monotonic preloadings. Only a few works investigated the influence of drained cyclic triaxial preloadings e.g. [36–38], and suggested that the liquefaction resistance increases with increasing the number of drained triaxial cycles in the preloadings stage. The literature is even scarcer regarding the influence of directional drained preloadings (instead of the typical drained triaxial compression/extension preloading). In particular, the recent work by Pan et al. [1] demonstrated that p−constant compression/extension drained preloadings alter the subsequent cyclic response and liquefaction resistance. In this work, however, only two directions were tested and the other possible different directional preloadings and drained triaxial compression were not considered. In addition, as experimentally demonstrated in London clay by Atkinson et al. [12] and Clayton & Heymann [39]; and on Toyoura and Fujian sands by Hong et al. [40] and Wang et al. [41,42], respectively, directional drained preloadings lead to a major influence on the maximum shear modulus and its subsequent degradation, and therefore, in its cyclic response and

---

* Corresponding author at: Universidad de la Costa, Barranquilla, Colombia.
E-mail address: jduque@cuc.edu.co (J. Duque).

liquefaction resistance. The aforementioned evidence suggest that there is a gap in the literature regarding the influence of directional drained cyclic preloadings on the subsequent liquefaction resistance and that more research is needed, which is the main goal of this article.

This article presents a detailed experimental investigation of the influence of directional drained cyclic preloadings on the subsequent undrained monotonic and cyclic response of Zbraslav sand. The experiments were performed considering different preloading directions, magnitude of the maximum deviatoric stress reached during the drained preloading stage and deviatoric stress amplitudes of the undrained shearing stage. The experimental results suggested that the preloading direction plays a major role on the contractive/dilative response during the subsequent undrained monotonic loading. In addition, the rate of strains and pore water pressure accumulation, and therefore, the number of cycles to reach initial liquefaction (i.e. to reach $r_u = u_w^{acc}/p_0 \approx 1$ for the first time) or failure conditions, where failure is hereafter defined as a single-amplitude of axial strain of $\varepsilon_1^{SA} = 10\%$, are remarkably affected by the direction of the drained preloading history. The results suggest that these major variations cannot be associated to the rather small changes in the relative density of the samples but likely due to fabric changes and induced anisotropy caused by the drained preloading history.

The structure of the article is as follows: first, a brief description of the properties and characteristics of Zbraslav sand is presented. Afterwards, a set of conventional undrained cyclic triaxial tests were performed to characterize the undrained cyclic resistance of Zbraslav sand. Finally, several undrained cyclic triaxial tests were performed considering different types of directional drained cyclic preloadings to investigate their influence on the subsequent undrained monotonic and cyclic response. The experimental data presented in the article will be uploaded at the soilmodels.com website [43].

2. Material description and samples preparation

All the experiments presented in the article were performed on Zbraslav sand, which is a common testing material from Prague, Czech Republic (e.g. [44–51], just to mention a few references). Some of the main characteristics of Zbraslav sand can be summarized as follows: mainly composed of quartz, grains with subangular shape, minimum and maximum void ratios of $e_{min} = 0.520$ and $e_{max} = 0.893$, coefficients of uniformity and curvature of $C_u = 3.19$ and $C_c = 0.98$, and critical state friction angle $\varphi_c = 34°$. Its grain size distribution is presented in Fig. 1. The adopted material is classified as a poorly graded sand (SP) according to the Unified Soil Classification System (USCS).

For the samples preparation, the procedure detailed by Wichtmann et al. [52] was adopted. For that purpose, the dry Zbraslav sand was carefully deposited in its loosest state and was subsequently compacted by tapping to achieve the desired initial relative density. The saturation procedure for triaxial samples is analogous to the one reported by Wichtmann [53] and Lade [54]. Initially, dry samples were placed in the triaxial cell and were saturated with CO_2. Then, the back and cell pressures were increased to 10 and 20 kPa, respectively. Under these stresses, samples were saturated with distilled deaerated water (i.e. we let deaerated water flow through the sample under these stresses very carefully, in order not to change the stress states). Subsequently, the back and cell pressures were gradually increased to 500 and 510 kPa, respectively. Finally, we again let flow distilled deaerated water through the sample under this back pressure. The aforementioned procedure always provided Skempton's coefficient $B \geq 0.99$, which confirms a full water-saturation [55]. In total, the full procedure for saturating dry sand samples placed in the triaxial cell takes 2 days. After the saturation, samples were isotropically consolidated at the corresponding initial mean effective stress of each test. A more detailed procedure followed for samples' preparation and characterization of Zbraslav sand can be found in [50].
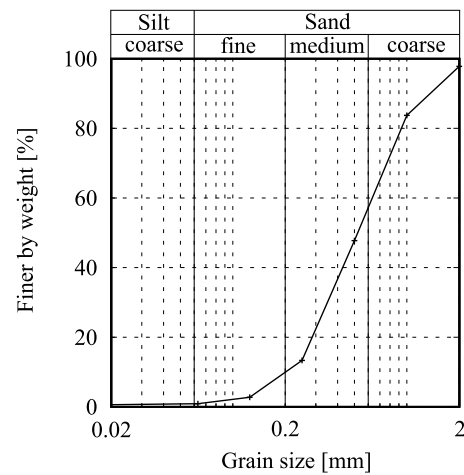

Fig. 1. Grain size distribution of Zbraslav sand.

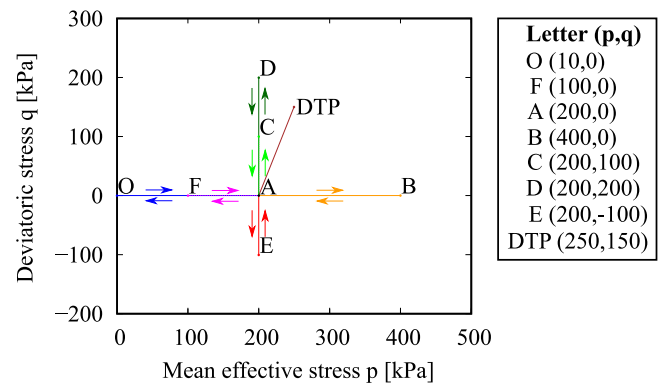| Letter (p,q) |
|---|
| O (10,0) |
| F (100,0) |
| A (200,0) |
| B (400,0) |
| C (200,100) |
| D (200,200) |
| E (200,-100) |
| DTP (250,150) |

Fig. 2. Evaluated preloading stress paths.

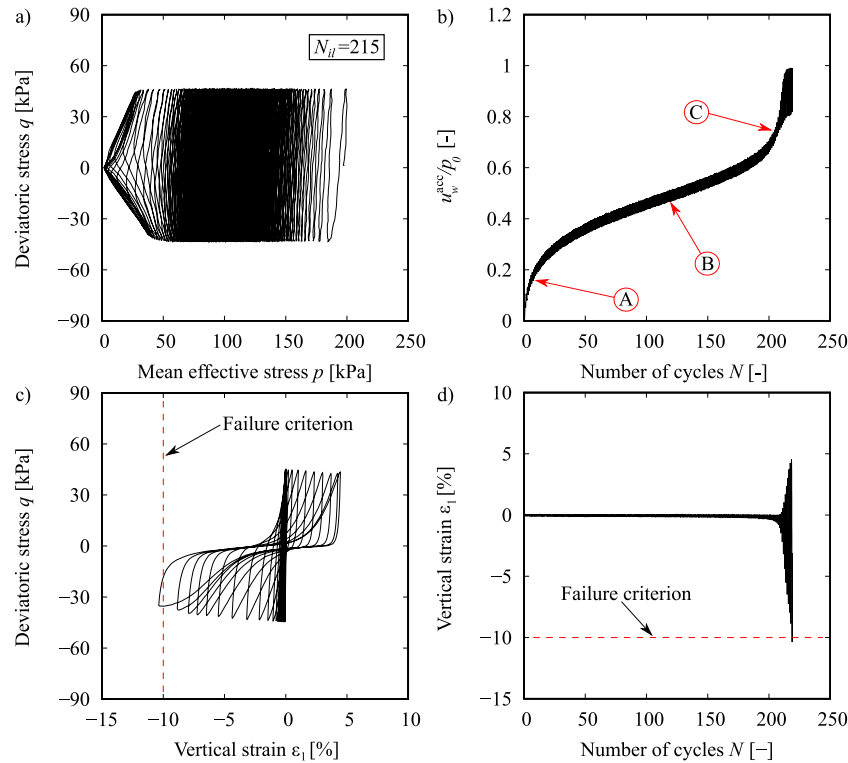## 3. Undrained cyclic triaxial tests

Twenty undrained cyclic triaxial tests were performed considering different deviatoric stress amplitudes $q^{amp} = (q^{max} - q^{min})/2$ and stress histories. Table 1 follows the nomenclature from the former work by Duque [50] and summarizes the detailed characteristics of each set of undrained cyclic triaxial tests. In particular, the table remarks the initial void ratio $e_{0_{bp}}$ and relative density $D_{r_{bp}}$ before the preloading stage (i.e. stress path O-A); initial void ratio e_0 and relative density D_r after the preloading stage (i.e. prior to the undrained shearing stage); mean effective stress p_0; deviatoric stress amplitude q^{amp}; Cyclic Stress Ratio (CSR = $q^{amp}/(2p_0)$); preloading history (see Fig. 2); number of cycles to reach initial liquefaction N_{il} (i.e. to reach $r_u = u_w^{acc}/p_0 \approx 1$ for the first time) and number of cycles to reach the failure criterion N_f. All undrained cyclic tests were performed on dense samples (relative density of $D_r \approx 70\%$). The undrained cyclic stages were performed with a stress-controlled approach and considering a sinusoidal waveform, with amplitude of q^{amp}, loading frequency of $f = 0.1$ Hz and period of T = 10 seconds. The selected loading frequency of 0.1 Hz correspond to typical offshore conditions [36,56–62].

The considered directional drained cyclic preloadings are summarized in Fig. 2 and are explicitly indicated in Table 1. Note that they include different preloading directions, and for some specific directions, different magnitude of the maximum deviatoric stress reached during the preloading stage. In particular, the drained preloadings paths were performed toward isotropic compression (stress path A–B), isotropic unloading (stress path A–F), p-constant compression (stress paths A–C and A–D), p-constant extension (stress path A–E) and drained triaxial compression (stress path A-DTP). Succeeding the aforementioned

Table 1
Programme of undrained cyclic triaxial tests.

Test name	$e_{0_{bp}}$ [-]	$D_{r_{bp}}$ [%]	e_0 [-]	D_r [%]	p_0 [kPa]	q^{amp} [kPa]	CSR [-]	Preloading path [-]	N_{il} [-]	N_f [-]
UCT1	–	–	0.625	71.95	200	45	0.1125	O-A	215	220
UCT2	–	–	0.634	69.48	200	50	0.125	O-A	138	143
UCT3	–	–	0.650	65.18	200	60	0.150	O-A	18	21
UCT4	–	–	0.640	67.83	200	70	0.175	O-A	6	11
UCT15	0.636	69.06	0.633	69.95	200	47	0.1175	O-A-C-A	252	260
UCT16	0.637	68.70	0.634	69.37	200	60	0.150	O-A-C-A	31	36
UCT17	0.631	70.26	0.628	71.04	200	70	0.175	O-A-C-A	11	15
UCT18	0.636	68.88	0.626	71.76	200	50	0.125	O-A-D-A	198	207
UCT19	0.627	71.43	0.620	73.28	200	60	0.150	O-A-D-A	69	78
UCT20	0.626	71.72	0.616	74.35	200	70	0.175	O-A-D-A	14	20
UCT21	0.624	72.26	0.618	73.87	200	50	0.125	O-A-E-A	460	470
UCT22	0.626	71.54	0.622	72.75	200	60	0.150	O-A-E-A	111	121
UCT23	0.630	70.67	0.624	72.16	200	70	0.175	O-A-E-A	36	43
UCT24	0.629	70.93	0.619	73.57	200	50	0.125	O-A-B-A	1341	1349
UCT25	0.629	70.73	0.620	73.26	200	60	0.150	O-A-B-A	261	268
UCT26	0.627	71.28	0.620	73.34	200	70	0.175	O-A-B-A	71	77
UCT27	0.635	69.21	0.635	69.29	200	50	0.125	O-A-F-A	107	113
UCT28	0.623	72.55	0.622	72.62	200	60	0.150	O-A-F-A	19	24
UCT29	0.627	71.33	0.627	71.43	200	70	0.175	O-A-F-A	8	13
UCT30	0.625	71.85	0.618	73.73	200	70	0.175	O-A-DTP†	11	17

DTP†: Drained triaxial preloading up to $q^{max}_{preloading} = 150$ kPa.

Fig. 3. Results of the undrained cyclic triaxial test UCT1 with isotropic consolidation ($p_0 = 200$ kPa, $q_0 = 0$) and deviatoric stress amplitude of $q^{amp} = 45$ kPa.

stages, the material was returned to the stress state A ($p_0 = 200$ kPa and $q = 0$). After the drained preloading stage, undrained cyclic shearing was performed considering symmetric deviatoric stress amplitudes.

3.1. Conventional undrained cyclic triaxial tests with variation of the deviatoric stress amplitude

Initially, four undrained cyclic triaxial tests UCT1–UCT4 were performed on samples with isotropic consolidation (stress path O-A) considering variation of the deviatoric stress amplitude 45 kPa $\leq q^{amp} \leq$ 70 kPa. The isotropic consolidation ended up in the stress states $\sigma_1 =$

$\sigma_2 = \sigma_3 = 700$ kPa and $u_w = 500$ kPa ($\sigma'_1 = \sigma'_2 = \sigma'_3 = 200$ kPa), or equivalently, $p_0 = 200$ kPa and $q_0 = 0$ kPa. A typical result (test UCT1) is presented in Fig. 3. The results show butterfly-shaped effective stress paths in the cyclic mobility phase, see Fig. 3a. The rate of pore water pressure accumulation exhibit three different stages ("A", "B" and "C") in which the pore water pressure accumulation presents a fast-slow-fast rates, see Fig. 3b. On the other hand, the results in the stress–strain space are presented in Fig. 3c and suggest that the accumulation of axial strains slowly grows up to the stage "C", after which ε_1^{amp} rapidly evolves in each subsequent cycle until failure conditions (i.e. single-amplitude of axial strain of $\varepsilon_1^{SA} = 10\%$) are achieved, see Fig. 3d. In addition, the results in the stress–strain space show an asymmetric
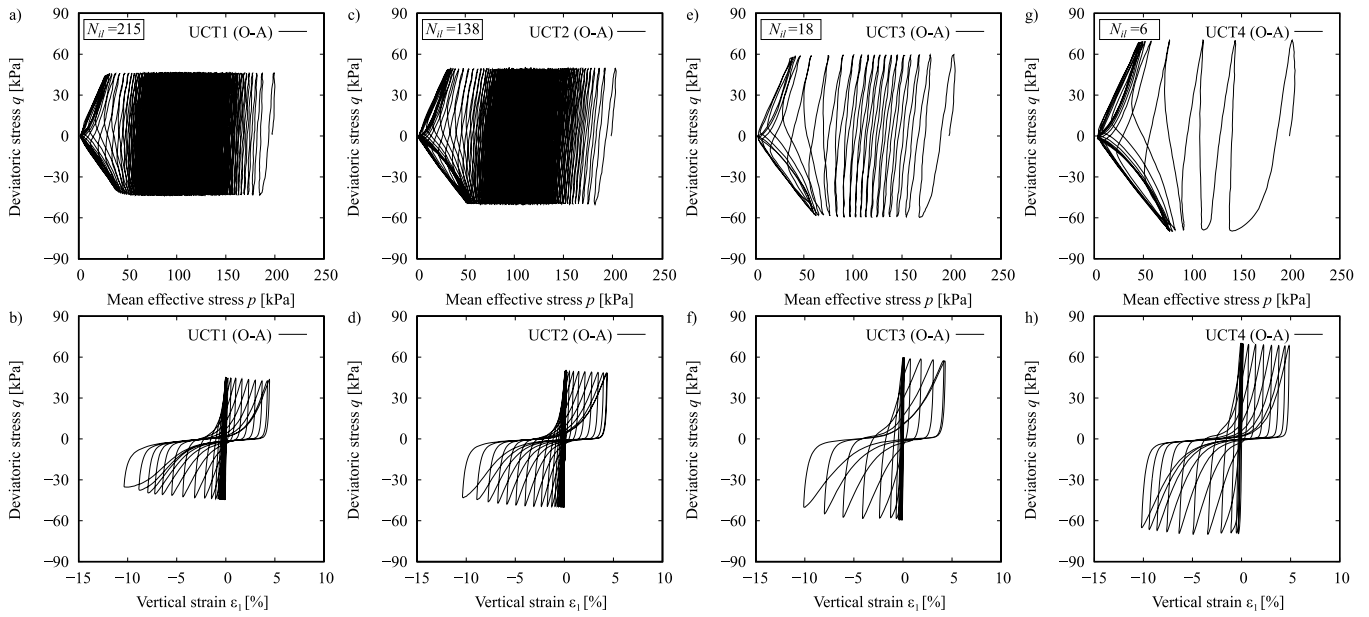
Fig. 4. Undrained cyclic triaxial tests UCT1–UCT4 with isotropic consolidation ($p_0 = 200$ kPa, $q_0 = 0$) and variation of the deviatoric stress amplitude $q^{amp} = \{45, 50, 60, 70\}$ kPa.
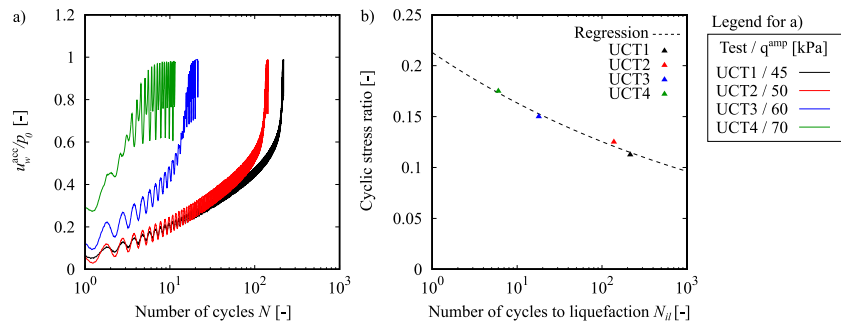

Fig. 5. Summary of undrained cyclic triaxial tests UCT1–UCT4 with isotropic consolidation (stress path O-A with $p_0 = 200$ kPa, $q_0 = 0$) and variation of the deviatoric stress amplitude $q^{amp} = \{45, 50, 60, 70\}$ kPa: (a) normalized accumulated pore water pressure u_w^{acc}/p_0 against the number of cycles N, (b) cyclic stress ratio CSR against the number of cycles to reach initial liquefaction N_{il}.

vertical strain accumulation in the extension side compared with the compression side that is in agreement with several former experimental observations e.g. [38,53,63–65].

The results of tests UCT1–UCT4 are summarized in Figs. 4 and 5. They show a significant increment in the accumulation rate of pore water pressure, and consequently, a reduction in the number of cycles to reach initial liquefaction with increasing deviatoric stress amplitude. Notice for example that test UCT1 with $q^{amp} = 45$ kPa required $N_{il} = 215$ and is contrasted with test UCT4 with $q^{amp} = 70$ kPa where $N_{il} = 6$. The relation between the cyclic stress ratio and the number of cycles to reach initial liquefaction for a given sand and density can be described using an equation of the form $CSR = aN_{il}^b$, where a and b are constants to be calibrated [38,53,56,66]. In particular, on medium dense samples of Zbraslav sand the constants $a = 0.2129$ and $b = -0.115$ hold. The potential function fairly well described the experiments, see Fig. 5b. The observed results on undrained cyclic triaxial tests are in accordance with many former experimental results e.g. [63,67–74].

3.2. Undrained cyclic triaxial tests with directional drained cyclic preloadings

Figs. 6 and 7 summarize the results of the undrained cyclic triaxial tests with and without directional drained cyclic preloadings, see Table 1 and Fig. 2 for details. Initially, Figs. 6a–c and 7a–c present the results of tests UCT2–UCT4 with isotropic consolidation (stress path O-A) as a benchmark. On the other hand, Figs. 6d–f and 7d–f present the results of tests UCT15–UCT17 in the $q - p$ and $q - \varepsilon_1$ spaces, respectively. Tests UCT15–UCT17 presented a p–constant compression drained preloading (i.e. stress path O-A-C-A). Some experimental observations of tests UCT15–UCT17 and their contrast with regard to tests UCT2–UCT4 are worthy to be remarked: (i) in the first quarter of the first cycle, which is actually a monotonic loading (i.e. it still does not presents any loading reversal) the material exhibits a more dilative response; (ii) the results show that after the first half of the first cycle there is almost negligible pore water pressure accumulation (i.e. no reduction of the mean effective stress); (iii) the rate of the reduction of the mean effective stress, or equivalently, the pore water pressure accumulation rate is reduced, which turns in higher number of cycles to reach initial liquefaction and failure conditions.

Tests UCT18–UCT20 were also performed considering a p–constant compression drained preloading but with a higher magnitude of the maximum deviatoric stress reached during the drained preloading stage (stress path O-A-D-A). The results are actually similar to those observed on tests UCT15–UCT17 but with the following main differences: (i) the dilative tendency within the first quarter of the first cycle was stronger; (ii) the first and second quarter of the first cycle (e.g. loading/unloading in the compression side) approximately follow the same effective stress path which renders in null mean effective stress reduction (i.e. pore water pressure accumulation); (iii) lower pore water pressure and strains
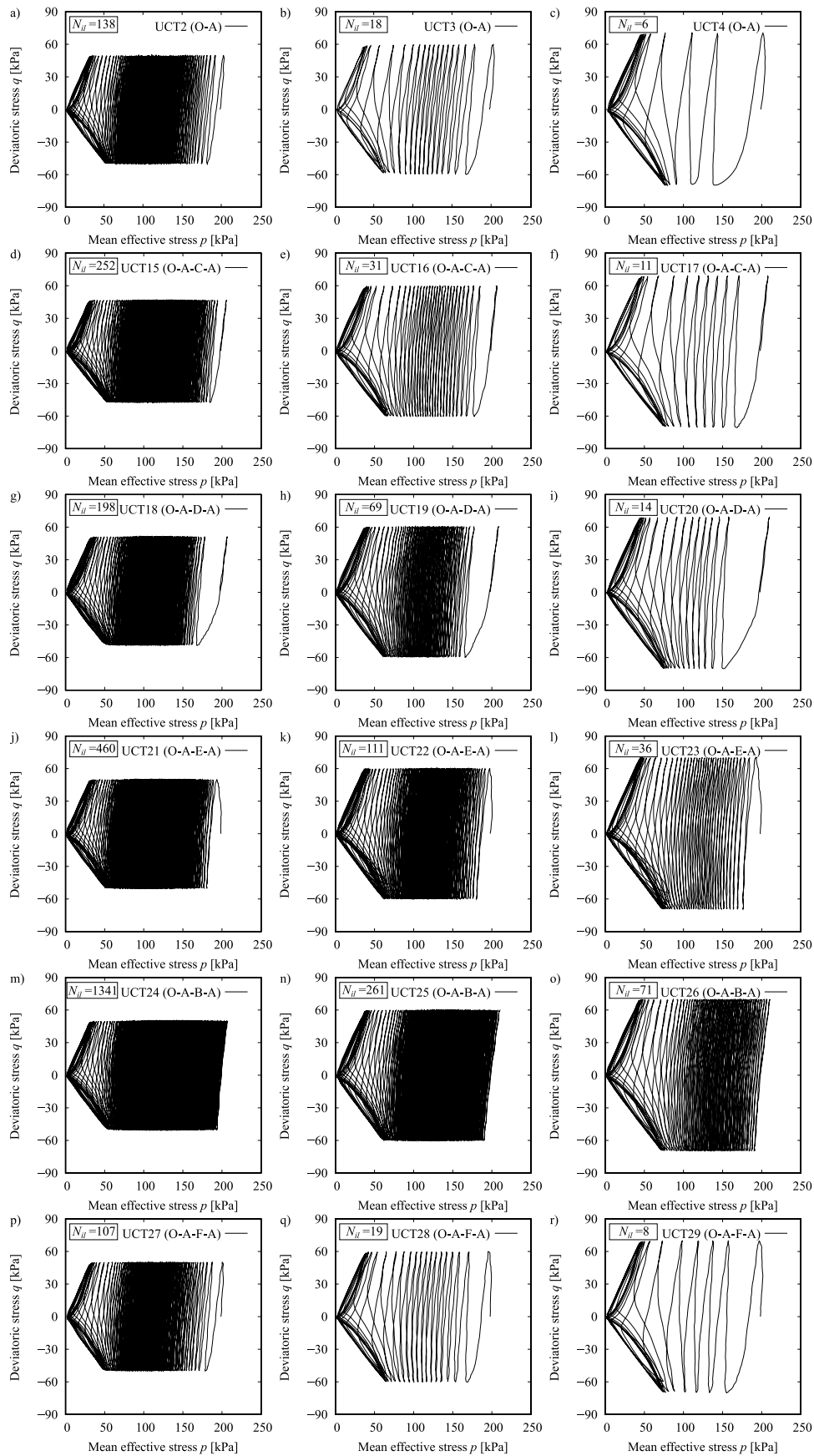
Fig. 6. Undrained cyclic triaxial tests with different stress histories: (a–c) O-A, (d–f) O-A-C-A, (g–i) O-A-D-A, (j–l) O-A-E-A, (m–o) O-A-B-A, (p–r) O-A-F-A.

Fig. 7. Undrained cyclic triaxial tests with different stress histories: (a–c) O-A, (d–f) O-A-C-A, (g–i) O-A-D-A, (j–l) O-A-E-A, (m–o) O-A-B-A, (p–r) O-A-F-A.
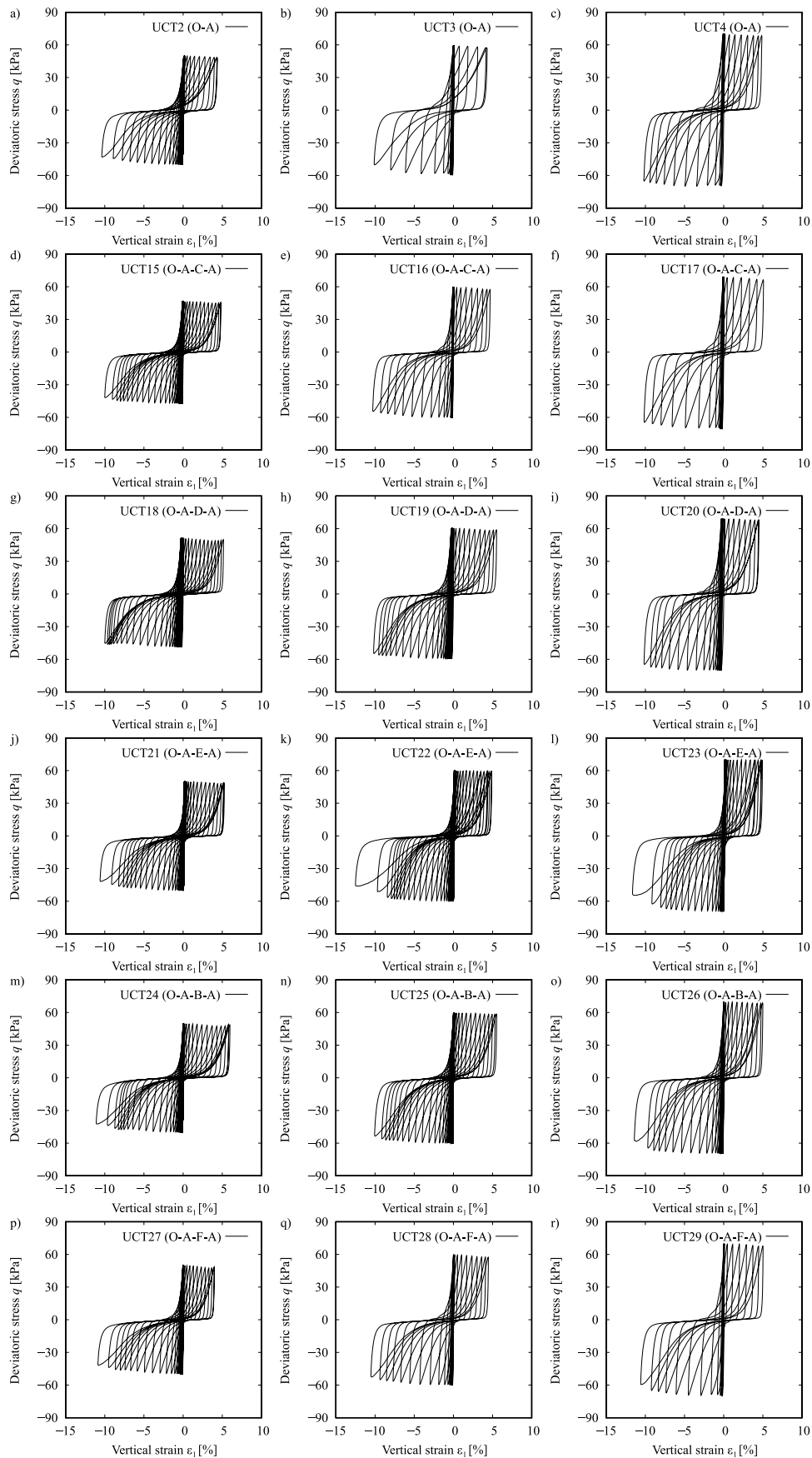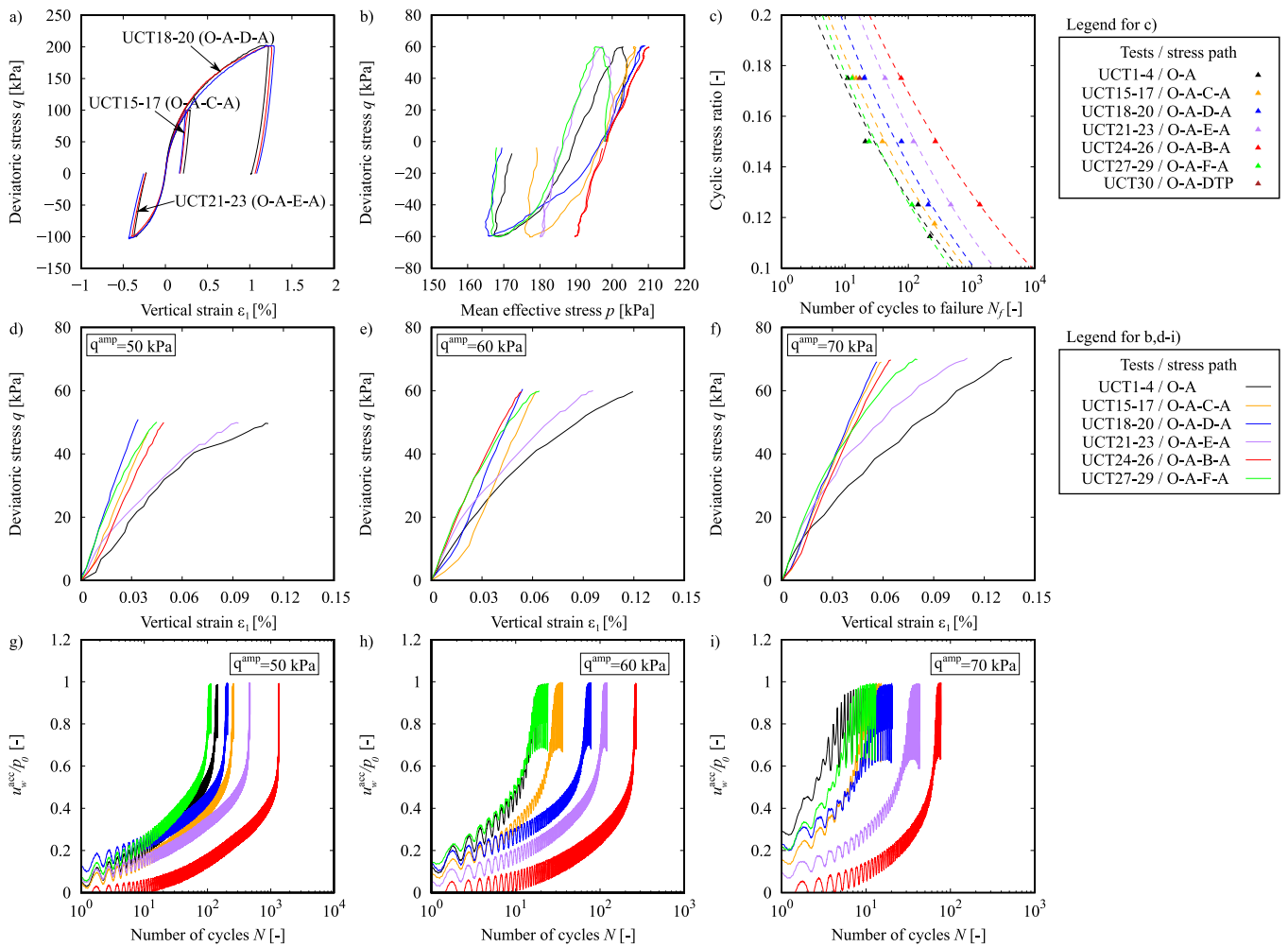
Fig. 8. Summary of undrained cyclic triaxial tests considering different stress histories prior to the undrained cyclic shearing: (a) vertical strain ε_1 against the deviatoric stress q during the preloading stage for tests UCT15–UCT23, (b) mean effective stress p against the deviatoric stress q in the first cycle of tests with deviatoric stress amplitude $q^{amp} = 60$ kPa, (c) cyclic stress ratio CSR against the number of cycles to reach failure conditions N_f, (d–f) deviatoric stress q against the vertical strain ε_1 obtained during the first quarter of cycle, (g–i) normalized accumulated pore water pressure u_w^{acc}/p_0 against the number of cycles N.

accumulation rates; (iv) increase in the number of cycles to reach initial liquefaction and failure conditions.

Figs. 6j–l and 7j–l present the results of tests UCT21–UCT23 in the $q - p$ and $q - \varepsilon_1$ spaces, respectively. The aforementioned tests were subjected to a p−constant extension drained preloading (i.e. stress path O-A-E-A). The comparison of tests UCT21–UCT23 with tests UCT2–UCT4 suggest the following main differences: (i) in the first quarter of the first cycle the material exhibits a more contractive response; (ii) the rate of pore water pressure accumulation is highly reduced, which turns in higher number of cycles to reach initial liquefaction and failure conditions; (iii) there is a small reduction in the vertical strain accumulation rate in the cyclic mobility phase (i.e. many additional mobilized cycles were needed to reach the same failure criterion of single-amplitude of axial strain of $\varepsilon_1^{SA} = 10\%$).

Tests UCT24–UCT26 were performed considering an isotropic compression preloading (i.e. stress path O-A-B-A). Figs. 6m–o and 7m–o present the results of the above-mentioned tests in the $q - p$ and $q - \varepsilon_1$ spaces, respectively. Some experimental observations of tests UCT24–UCT26 and their contrast with regard to tests UCT2–UCT4 deserve to be remarked: (i) there is almost negligible mean effective stress reduction in the first cycle; (ii) the rate of the mean effective stress reduction is extremely lower, which turns in higher number of cycles to reach initial liquefaction and failure conditions; (iii) due to the extreme reduction in the accumulation rates, the qualitative shape of the pore water pressure accumulation against the number of cycles curve is different,

see Fig. 8g–i; (iv) the material exhibits a small reduction in the vertical strain accumulation in the cyclic mobility phase. Finally, Figs. 6m–o and 7m–o present the results of tests UCT27–UCT29 with preloading stress path O-A-F-A. A slightly more contractive response was observed in the first quarter of the first cycle. Apart from that, the results are very similar to those observed on tests UCT2–UCT4.

The summary of the previously discussed experimental results is presented in Fig. 8. Initially, Fig. 8a shows the $q - \varepsilon_1$ space during the preloading stages of tests UCT15–UCT23. The results are pretty consistent with each other which confirms a high level of repeatability. Fig. 8b presents the mean effective stress p against the deviatoric stress q during the first cycle of tests with deviatoric stress amplitude $q^{amp} = 60$ kPa (for schematic purposes) and different preloading directions. In comparison to the test without preloading (UCT3), the tests with preloading paths toward p−constant extension (i.e. stress path O-A-E-A) produce a more contractive response in the first quarter of the first cycle, tests with drained preloadings toward p−constant compression and isotropic compression (i.e. stress paths O-A-C-A, O-A-D-A and O-A-B-A, respectively), produce a more dilative behaviour. On the other hand, Figs. 8d–f present the results of tests UCT15–UCT29 during the first quarter of cycle (i.e. monotonic path) in the $q - \varepsilon_1$ space. Consistent with the experimental results on London clay reported by Atkinson et al. [12], the tests without preloadings produce the lowest stiffness. The primarily continuous loading regarding subsequent undrained loading direction (i.e. stress path O-A-E-A) gives
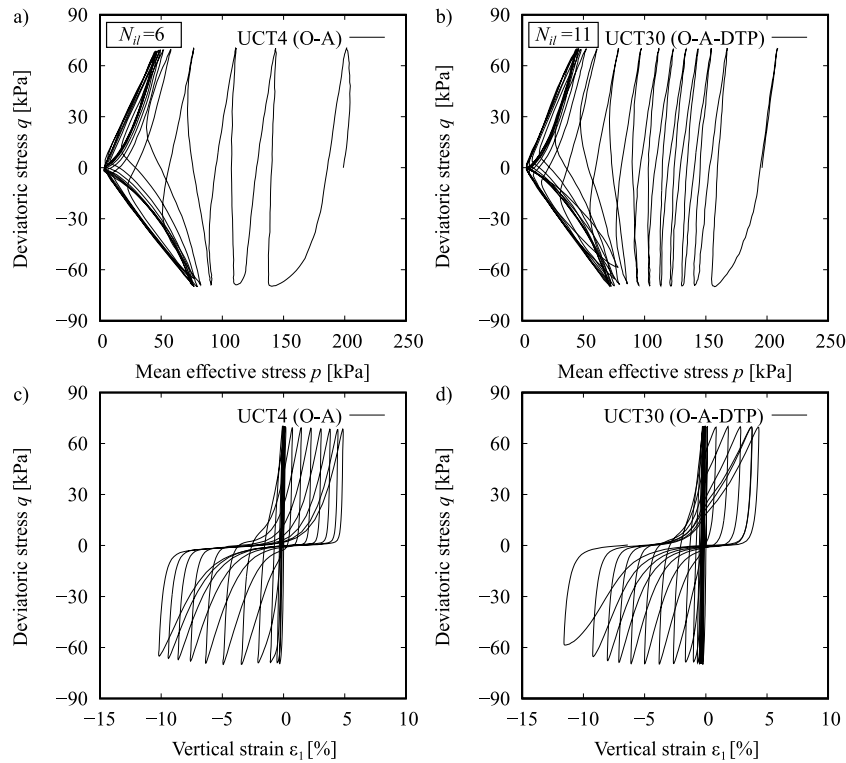
Fig. 9. Comparison of undrained cyclic triaxial tests UCT4 and UCT30 without and with drained triaxial compression preloading with $q^{\mathrm{max}}_{\mathrm{triaxialpreloading}}$ = 150 kPa, respectively, and deviatoric stress amplitude q^{amp} = 70 kPa.

very similar low stiffness. On the other hand, the four other cases are clearly stiffer. If the initial low stiffness of the test with preloading path O-A-D-A and deviatoric stress amplitude of 60 kPa is not considered (which is due to bedding effects), the tests with preloading paths O-A-D-A are the stiffest which is also consistent with the recent stress history theories (full reversal, larger magnitude) [12,40,41]. Unfortunately, more detailed information could not be measured since strains were not measured locally through Linear Variable Differential Transformers (LVDTs). Figs. 8g–i present the normalized accumulated pore water pressure u^{acc}_w/p_0 against the number of cycles N on the tests with different types of directional drained cyclic preloadings. It is clear that the test without preloading and the test with preloading O-A-F-A approximately follows the same $u^{\mathrm{acc}}_w/p_0 - N$ curve. The curves then need progressively more cycles to reach failure in the tests with preloadings toward the compression and extension side i.e. O-A-C-A, O-A-D-A and O-A-E-A, respectively. The slowest pore water pressure accumulation is observed on the test with isotropic compression preloading (i.e. stress path O-A-B-A). Finally, Fig. 8c presents the summary of the CSR − N_f curve for the different tests. The results suggest that tests with preloadings O-A-F-A approximately follows the same trend than tests without preloadings. The curve is then shifted (there is an increase in the number of cycles to reach failure) with approximately unchanged inclination on tests with preloadings toward p−constant compression, p−constant extension and isotropic compression, or equivalently, preloading paths O-A-C-A, O-A-D-A, O-A-E-A and O-A-B-A, respectively.

Former experimental studies on sands have shown that cyclic tests on samples with variation of relative densities of ±6% approximately follow the same CSR − N_f curve [38,56,64,75]. In particular, the performed tests with directional drained cyclic preloadings led to variations of relative densities lower than 3% (see Table 1). Therefore, the important differences in the accumulation rates and number of cycles to reach failure conditions is not associated with the small reductions of void ratios but rather may be attributed to induced anisotropy and changes in fabric in case of samples subjected to shearing preloadings.

On the other hand, the differences on samples subjected to isotropic compression preloadings are likely related to a combination of fabric change, induced anisotropy and crushing of grains due to the ratio between grain size and sample height.

3.3. Test with drained triaxial preloading

An additional test UCT30 with a preloading in an intermediate direction (a drained monotonic triaxial compression with $q^{\mathrm{max}}_{\mathrm{triaxialpreloading}}$ = 150 kPa) was performed to evaluate their influence on the subsequent undrained cyclic response. The preloading was only performed on the compression side. The results of tests UCT4 and UCT30 are presented in Fig. 9 and suggest that the result of test UCT30 is qualitatively similar to the one of tests with preloadings toward positive deviatoric stresses at constant mean effective stress presented in the previous section (stress paths O-A-C-A and O-A-D-A, where $q^{\mathrm{max}}_{\mathrm{preloading}}$ was 100 and 200 kPa, respectively). From a quantitative point of view, the number of cycles to reach failure conditions lies between the tests with preloading stress paths O-A-C-A and O-A-D-A, see Fig. 8c. A more detailed analysis of the influence of drained or undrained monotonic and cyclic triaxial preloadings on the liquefaction resistance is presented in [50].

4. Summary and conclusions

Different factors may induce preloading histories in in-situ sand deposits such as excavations, tunnelling, refilling, compaction and construction of overlying structures. The aforementioned preloadings stages modify the subsequent soil mechanical behaviour, and therefore, the ground deformations and liquefaction resistance. This article presented the results of an experimental programme devoted to investigate the influence of drained cyclic preloadings performed in different directions on the subsequent undrained cyclic response and liquefaction resistance of Zbraslav sand. The main conclusions of the study are summarized as:

- The experimental results suggested that the preloading direction plays an important role on the contractive/dilative response during the subsequent undrained monotonic loading. In particular, p−constant compression directional drained cyclic preloadings and isotropic compression (i.e. paths O-A-C-A, O-A-D-A and O-A-B-A) led to more dilative responses. On the other hand, p−constant extension directional drained cyclic preloadings (i.e. path O-A-E-A) led to more contractive responses.
- The influence of preloading on the shear stiffness of the sample during the first quarter of cycle (monotonic loading) is consistent with the known effect of recent stress history from the literature.
- Directional drained cyclic preloadings have a major effect on the cyclic response of coarse-grained soils. In particular, there is a remarkable influence of the directional drained cyclic preloadings in the pore water pressure accumulation such that the $CSR - N_f$ curve is progressively translated toward higher N_f with practically unchanged inclinations. In particular, directional drained cyclic preloadings with isotropic unloading (stress path O-A-F-A) led to almost identical number of cycles to reach failure conditions than tests without preloadings. Then, the number of cycles to reach failure conditions progressively increases on tests with paths toward p−constant compression, p−constant extension and isotropic compression (i.e. O-A-C-A, O-A-D-A, O-A-E-A and O-A-B-A), respectively. In other words, extension shear preloading induces more pronounced effects than compression shear preloading, while the effect of isotropic compression preloading is even more pronounced. The DTP test fits into the scheme, being between the results of tests with preloadings paths O-A-C-A and O-A-D-A.
- The remarkable variation in the accumulation rates and the number of cycles to reach liquefaction or failure conditions cannot be associated to the rather small changes in relative density of the samples but likely may be attributed to induced anisotropy and changes in fabric in case of samples subjected to shearing preloadings. On the other hand, the differences on samples subjected to isotropic compression preloadings are likely related to a combination of fabric change, induced anisotropy and crushing of grains due to the ratio between grain size and sample height.

The experimental data presented in the article will be uploaded at the soilmodels.com website [43], and is expected to be used for the validation and improvement of constitutive models on scenarios involving different types of cyclic preloadings.

Notation

Symbol	Name
B	Skempton's coefficient
C_c	coefficient of curvature
C_u	uniformity coefficient
CO_2	carbon dioxide
CSR	cyclic stress ratio
d	diameter
D_r	initial relative density
$D_{r_{bp}}$	initial relative density before the preloading
D_{50}	mean particles diameter
e	void ratio
e_0	initial void ratio
$e_{0_{bp}}$	initial void ratio before preloading
e_{max}	maximum void ratio

Symbol	Name
e_{min}	minimum void ratio
G_s	specific gravity
h	height
N	number of cycles
N_{il}	number of cycles to reach initial liquefaction
N_f	number of cycles to reach the failure criterion
p	mean effective stress
q	deviatoric stress
q^{amp}	deviatoric stress amplitude
r_u	pore water pressure ratio
T	period
u_w^{acc}	accumulated pore water pressure
u_w^{acc}/p_0	normalized accumulated pore water pressure
ε_1	axial strain
ε_1^{amp}	axial strain amplitude
ε_1^{SA}	single-amplitude of axial strain
φ_c	critical state friction angle
σ_3	total radial stress
σ_1	total axial stress
σ_3'	effective radial stress
σ_1'	effective axial stress

CRediT authorship contribution statement

J. Duque: Conceptualization, Methodology, Formal analysis, Validation, Writing – original draft. **J. Roháč:** Conceptualization, Methodology, Validation, Writing – review & editing. **D. Mašín:** Conceptualization, Methodology, Formal analysis, Writing – original draft, Supervision.

Declaration of competing interest

The authors declare that they have no known competing financial interests or personal relationships that could have appeared to influence the work reported in this paper.

Data availability

Data will be made available on request.

Acknowledgements

References

[1] Pan K, Cai Y, Yang Z, Pan X. Liquefaction of sand under monotonic and cyclic shear conditions: Impact of drained preloading history. Soil Dyn Earthq Eng 2019;126:105775.

[2] Duque J, Ochmański M, Mašín D, Hong Y, Wang L. On the behavior of monopiles subjected to multiple episodes of cyclic loading and reconsolidation in cohesive soils. Comput Geotech 2021;134.

[3] Duque J, Ochmański M, Mašín D. On the influence of multiple episodes of cyclic loading and reconsolidation on the behavior of monopiles embedded in fine-grained soils. In: IACMAG 2022: Challenges and innovations in geomechanics. Turin, Italy; 2022, p. 95–101.

[4] Liu Z, Xue J, Ye J. The effects of unloading on drained cyclic behaviour of Sydney sand. Acta Geotech 2021;16(9):2791–804.

[5] Toyota H, Takada S. Variation of liquefaction strength induced by monotonic and cyclic loading histories. J Geotech Geoenviron Eng 2017;143(4):04016120.

[6] Oda M, Kawamoto K, Suzuki K, Fujimori H, Sato M. Microstructural interpretation on reliquefaction of saturated granular soils under cyclic loading. J Geotech Geoenviron Eng 2001;127(5):416–23.

[7] Fuentes W, Mašín D, Duque J. Constitutive model for monotonic and cyclic loading on anisotropic clays. Géotechnique 2021;71(8):657–73.

[8] Duque J, Mašín D, Fuentes W. Improvement to the intergranular strain model for larger numbers of repetitive cycles. Acta Geotech 2020;15:3593–604.

[9] Stallebrass S. Modelling the effect of recent stress history on the deformation of overconsolidated soils [Ph.D. thesis], London, UK: City, University of London; 1990.

[10] Duque J, Yang M, Fuentes W, Mašín D, Taiebat M. Characteristic limitations of advanced plasticity and hypoplasticity models for cyclic loading of sands. Acta Geotech 2022;17:2235–57.

[11] Afifi S, Richart J. Stress-history effects on shear modulus of soils. Soils Found 1973;13(1):77–95.

[12] Atkinson J, Richardson D, Stallebrass S. Effect of recent stress history on the stiffness of overconsolidated soil. Géotechnique 1990;40(4):531–40.

[13] Stallebrass S, Taylor R. The development and evaluation of a constitutive model for the prediction of ground movements in overconsolidated clay. Géotechnique 1997;47(2):235–53.

[14] Duque J, Mašín D, Fuentes W. Hypoplastic model for clays with stiffness anisotropy. In: Proceedings of IACMAG 2021: Challenges and innovations in geomechanics. Turin, Italy; 2021, p. 414–21.

[15] Finn L, Bransby P, Pickering D. Effect of strain history on liquefaction of sand. J Soil Mech Found Div 1970;96(6):1917–34.

[16] Lee K, Albaisa A. Earthquake induced settlements in saturated sands. J Geotech Eng Div 1974;100(4):387–406.

[17] Toki S, Kitago S. Effects of repeated loading on deformation behavior of dry sand. Soils Found 1974;14(1):95–103.

[18] Ishihara K, Okada S. Effects of stress history on cyclic behavior of sand. Soils Found 1978;18(4):31–45.

[19] Ishihara K, Okada S. Effects of large preshearing on cyclic behavior of sand. Soils Found 1982;22(3):109–25.

[20] Suzuki T, Toki S. Effects of preshearing on liquefaction characteristics of saturated sand subjected to cyclic loading. Soils Found 1984;24(2):16–28.

[21] Sriskandakumar S, Wijewickreme S, Byrne P. Multiple cyclic loading response of loose air-pluviated fraser river sand. In: Proceedings of the 15th world conference on earthquake engineering. Lisbon, Portugal; 2012, p. 1–10.

[22] Vaid Y, Thomas J. Liquefaction and post liquefaction behavior of sand. J. Geotech Eng 1995;121(2):163–73.

[23] Seed H, Mori K, Chan C. Influence of seismic history on liquefaction of sands. J Geotech Eng Div 1977;103(4):257–70.

[24] Seed R, Lee S, Jong H. Penetration and liquefaction resistances: Prior seismic history effects. J Geotech Eng 1988;114(6):691–7.

[25] Sivathayalan S, Yazdi M. Influence of strain history on postliquefaction deformation characteristics of sands. J Geotech Geoenviron Eng 2014;140(3):04013019.

[26] Doanh T, Ibraim E, Matiotti R. Undrained instability of very loose Hostun sand in triaxial compression and extension. Part 1: Experimental observations. Mech Cohes-Frict Mater 1997;2(1):47–70.

[27] Dubujet P, Doanh T. Undrained instability of very loose Hostun sand in triaxial compression and extension. Part 2: Theoretical analysis using an elastoplasticity model. Mech Cohes-Frict Mater 1997;2(1):71–92.

[28] Doanh T, Dubujet P, Touron G. Exploring the undrained induced anisotropy of Hostun RF loose sand. Acta Geotech 2010;5(4):239–56.

[29] Doanh T, Finge Z, Boucq S, Dubujet P. Histotropy of Hostun RF loose sand. In: Modern trends in geomechanics. 2006, p. 399–411.

[30] Gajo A, Piffer L. The effects of preloading history on the undrained behaviour of saturated loose sand. Soils Found 1999;39(6):43–53.

[31] Bobei D, Wanatowski D, Rahman M, Lo S, Gnanendran C. The effect of drained pre-shearing on the undrained behaviour of loose sand with a small amount of fines. Acta Geotech 2013;8:311–22.

[32] Finge Z, Doanh T, Dubujet P. Undrained anisotropy of Hostun RF loose sand: New experimental investigations. Can Geotech J 2006;43(11):1195–212.

[33] Doanh T, Finge Z, Boucq S. Effects of previous deviatoric strain histories on the undrained behaviour of Hostun RF loose sand. Geotech Geol Eng 2012;30(4):697–712.

[34] Arab A, Sadek M, Belkhatir M, Shahrour I. Monotonic preloading effect on the liquefaction resistance of chlef silty sand: A laboratory study. Arab J Sci Eng 2014;39(2):685–94.

[35] Duque J, Roháč J, Mašín D, Najser J. Experimental investigation on Malaysian kaolin under monotonic and cyclic loading: Iinspection of undrained miner's rule and drained cyclic preloading. Acta Geotech 2022;17:4953–75.

[36] Andersen K. Cyclic soil parameters for offshore foundation design. In: Frontiers in offshore geotechnics III: Proceedings of the 3rd international symposium on frontiers in offshore geotechnics. Leiden; 2015, p. 5–82.

[37] Wichtmann T, Niemunis A, Triantafyllidis T, Poblete M. Correlation of cyclic preloading with the liquefaction resistance. Soil Dyn Earthq Eng 2005;25(12):923–32.

[38] Wichtmann T. Soil behaviour under cyclic loading: Experimental observations, constitutive description and applications. Habilitation, Karlsruhe Institute of Technology (KIT); 2016.

[39] Clayton C, Heymann G. Stiffness of geomaterials at very small strains. Géotechnique 2001;51(3):245–55.

[40] Hong Y, Koo C, Zhou C, Ng C, Wang L. Small strain path-dependent stiffness of Toyoura sand: Laboratory measurement and numerical implementation. Int J Geomech 2017;17(1):04016036.

[41] Wang L, Wang H, Zhu B, Hong Y. Comparison of monotonic and cyclic lateral response between monopod and tripod bucket foundations in medium dense sand. Ocean Eng 2018;155:88–105.

[42] Ochmański M, Mašín D, Duque J, Hong Y, Wang L. Performance of tripod foundations for offshore wind turbines: A numerical study. Géotech Lett 2021;11(3):230–8.

[43] Gudehus G, Amorosi A, Gens A, Herle I, Kolymbas D, Mašín D, et al. The soilmodels.info project. Int J Numer Anal Methods Geomech 2008;32(12):1571–2.

[44] Mašín D. Incorporation of meta-stable structure into hypoplasticity. In: Proceedings of the international conference on numerical modelling of construction processes in geotechnical engineering for urban environment. Bochum, Germany; 2006, p. 283–90.

[45] Feda J. Základy mechaniky partikulárních látek. Prague: Československá akademie věd; 1977.

[46] Herle I, Gudehus G. Determination of parameters of a hypoplastic constitutive model from properties of grain assemblies. Mech Cohes-Frict Mater 1999;4(5):461–86.

[47] Feda J. Notes on the effect of grain crushing on the granular soil behaviour. Eng Geol 2002;63(1–2):93–8.

[48] Feda J. Mechanics of particulate materials, the principles. Prague: Elsevier Science; 1982.

[49] Feda J. Stress-path dependent shear strength of sand. J Geotech Eng 1994;120(6):958–74.

[50] Duque J. Contributions to the experimental investigation and numerical description of soil cyclic behavior [Ph.D. thesis], Prague, Czech Republic: Charles University; 2021.

[51] Boháč J, Feda J. Membrane penetration in triaxial tests. Geotech Test J 1992;15(3):288–94.

[52] Wichtmann T, Steller K, Triantafyllidis T. On the influence of the sample preparation method on strain accumulation in sand under high-cyclic loading. Soil Dyn Earthq Eng 2020;131:106028.

[53] Wichtmann T. Explicit accumulation model for non-cohesive soils under cyclic loading [Ph.D. thesis], Germany: Ruhr-Universität Bochum; 2005.

[54] Lade P. The stress-strain and strength characteristics of cohesionless soils [Ph.D. thesis], University of California, Berkeley; 1972.

[55] Head K. Manual of soil laboratory testing. Volume 3: Effective stress tests. 2nd ed.. John Wiley & Sons; 1998.

[56] Wichtmann T, Triantafyllidis T. An experimental data base for the development, calibration and verification of constitutive models for sand with focus to cyclic loading. Part I: Tests with monotonic loading and stress cycles. Acta Geotech 2016;11(4):739–61.

[57] Li L, Dan H, Wang L. Undrained behavior of natural marine clay under cyclic loading. Ocean Eng 2011;38(16):1792–805.

[58] Vinck K, Liu T, E. U, Jardine R. An appraisal of end conditions in advanced monotonic and cyclic triaxial testing on a range of geomaterials. In: 7th International Symposium on Deformation Characteristics of Geomaterials, Vol. 92. 2019.

[59] Zografou D. Investigation of shallow skirted foundations under undrained cyclic loading [Ph.D. thesis], University of Western Australia; 2018.

[60] Son S, Yoon J, Kim J. Simplified method for defining 2-dimensional design failure curve of marine silty sand under dynamic loading. J Mar Sci Eng 2020;8(1):1–15.

[61] Blaker O, Andersen K. Shear strength of dense to very dense dogger bank sand. In: Frontiers in offshore geotechnics III: Proceedings of the 3rd international symposium on frontiers in offshore geotechnics. Leiden; 2015, p. 1167–72.

[62] Blaker O, Andersen K. Cyclic properties of dense to very dense silica sand. Soils Found 2019;59(4):982–1000.

[63] Hyodo M, Hyde A, Aramaki N. Liquefaction of crushable soils. Géotechnique 1998;48(4):527–43.

[64] Parra A. Ottawa F-65 sand characterization [Ph.D. thesis], Davis: University of California; 2016.

[65] Ueda K, Vargas R, Uemura K. LEAP-Asia-2018: Stress-strain response of Ottawa sand in cyclic torsional shear tests. DesignSafe-CI 2018.

[66] Fuentes W. Contributions in mechanical modelling of fill materials [Ph.D. thesis], Germany: Karlsruhe Institute of Technology; 2014.

[67] Ghionna V, Porcino D. Liquefaction resistance of undisturbed and reconstituted samples of a natural coarse sand from undrained cyclic triaxial tests. J Geotech Geoenviron Eng 2006;132(2):194–202.

[68] Yang J, Sze H. Cyclic behaviour and resistance of saturated sand under non-symmetrical loading conditions. Géotechnique 2011;61(1):59–73.

[69] Yang J, Sze H. Cyclic strength of sand under sustained shear stress. J Geotech Geoenviron Eng 2011;137(12):1275–85.

[70] Fuentes W, Gil M, Duque J. Dynamic simulation of the sudden settlement of a mine waste dump under earthquake loading. Int J Min, Reclam Environ 2019;33(6):425–43.

[71] Sharma S, Ismail M. Monotonic and cyclic behavior of two calcareous soils of different origins. J Geotech Geoenviron Eng 2006;132(12):1581–91.

[72] Wijewickreme D, Sriskandakumar S, Byrne P. Cyclic loading response of loose air-pluviated Fraser river sand for validation of numerical models simulating centrifuge tests. Can Geotech J 2005;42(2):550–61.

[73] Vaid Y, Chung E, Kuerbis R. Preshearing and undrained response of sand. Soils Found 1989;29(4):49–61.

[74] Vaid Y, Chern J. Effect of static shear on resistance to liquefaction. Soils Found 1983;23(1):47–60.

[75] Wichtmann T, Triantafyllidis T. An experimental data base for the development, calibration and verification of constitutive models for sand with focus to cyclic loading. Part II: Tests with strain cycles and combined loading. Acta Geotech 2016;11(4):763–74.